NANO LETTERS

2009
Vol. 9, No. 7
2715-2718

# Electron-Beam-Induced Deposition of Platinum from a Liquid Precursor

**Eugenii U. Donev and J. Todd Hastings***

*Department of Electrical and Computer Engineering, University of Kentucky, Lexington, Kentucky 40506*

*Received April 16, 2009; Revised Manuscript Received June 1, 2009*

## ABSTRACT

**We demonstrate here the first focused electron-beam-induced deposition (EBID) of nanostructures using a liquid precursor. We have deposited sub-50 nm platinum (Pt) wires and dots from a dilute, aqueous solution of chloroplatinic acid. Existing EBID processes rely on the electron-beam stimulated decomposition of gaseous precursors; as a result, the deposits are highly contaminated (up to 75 at. % carbon or 60 at. % phosphorus for Pt processes). In contrast, we show that deposition of platinum by electron-beam reduction of platinum ions from solution leads to high-purity deposits (~10 at. % chlorine contamination) at rates at least ten times higher than those obtained with other platinum precursors. Liquid-phase EBID offers a new route to deterministic, three-dimensional, nanometer-scale structures composed of multiple materials without complex multistep processing. Thus, it may prove important for prototyping and low-volume production of nanoscale devices and for repair and modification of nanoscale masks and templates used in high-volume production.**



Focused electron-beam-induced deposition (EBID) allows the direct formation of nanostructures through localized electron-beam induced decomposition of adsorbed gas precursors. EBID has been widely investigated for nanoscale device prototyping (e.g., field emission arrays,[1,2] electrical connections to nanowires and nanotubes,[3,4] and patterned catalyst deposition[5,6]) and for lithographic mask repair in integrated-circuit manufacturing.[7,8] Closely related processes have also been developed using focused ion beams and have been used for complex three-dimensional nanofabrication and semiconductor mask repair.[9] These processes allow deposition of certain metals, magnetic materials, semiconductors, and insulators with varying degrees of purity.[8−10] However, gas-phase EBID has many limitations including a single reaction mechanism (decomposition), the use of toxic, reactive, and expensive precursors, charging of nonconductive substrates, and, perhaps most importantly, low purity of the deposits. In contrast, the liquid-phase (LP) EBID method demonstrated in the present work promises a wider variety of precursors and deposition reactions, the use of more stable, inexpensive, and benign precursors, higher deposition rates, charge dissipation when using conductive solutions, and, perhaps most importantly, high-purity deposits.

To assess the feasibility of LP-EBID, we investigated the deposition of platinum (Pt) from 1% (by weight) chloroplatinic acid ($H_2PtCl_6$, Sigma-Aldrich Inc.) in deionized (18 MΩ) water. Depositions were carried out in QuantomiX QX-102 WETSEM capsules, which separate a liquid from the vacuum chamber using a thin (~150 nm) polyimide membrane.[11] Colloidal gold nanoparticles (Au NPs) were used as focusing artifacts on the membrane. As shown in Figure 1, Pt was deposited on the membrane itself by focusing the electron beam at the liquid-membrane interface. To assess the resolution of the process, we exposed single-pixel dots, separated by 1 $\mu$m, at doses ranging from 2 to 27 pC. Several arbitrary patterns, such as the four-wire measurement structure shown in Figure 1c, were also deposited. Larger features, 2 $\mu$m × 2 $\mu$m regions of dots spaced by 200 nm, were deposited to determine the composition of the deposited material. For these regions, an areal dose of 35 mC/cm$^2$ was used. All depositions were carried out using a primary beam energy of 20 keV and a beam current of 200 pA in a Raith e_LiNE electron-beam lithography tool. A control experiment was conducted with a capsule filled only with the QuantomiX imaging buffer solution. The exposure process was repeated, but no deposition of any type was observed in the control capsule even when doses were increased up to 50 times higher than the required dose for the $H_2PtCl_6$ solution.

Scanning electron micrographs (SEMs) were taken in situ (i.e., through the membrane) immediately after patterning. No deposition was observed at the electron doses required for imaging. The capsules were then opened, the $H_2PtCl_6$ solution was aspirated, and the membranes were flushed ten times with deionized water to remove any residual $H_2PtCl_6$. After drying, ex situ SEMs were taken of deposited features on the underside of the membrane (the side formerly in contact with the solution). The larger area deposits were also characterized ex situ using energy-dispersive X-ray spectroscopy on a Hitachi S-3200 SEM. Finally, the membranes

* Corresponding author, hastings@engr.uky.edu.

10.1021/nl9012216 CCC: $40.75 
**Published on Web 06/11/2009**

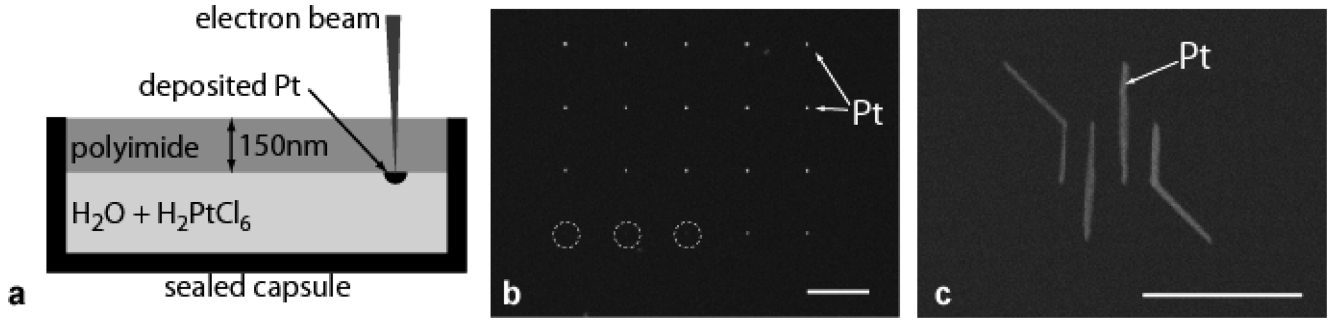


**Figure 1.** (a) Schematic of liquid-phase electron-beam-induced deposition (LP-EBID) of platinum from chloroplatinic acid solution. The solution is separated from the vacuum system by a polyimide membrane and the electron beam is focused at the membrane−solution interface to induce deposition. (b) In situ electron micrograph of Pt nanodots deposited by LP-EBID. The dose increases from lower left to upper right. Scale bar indicates 1 $\mu$m. (c) Ex situ electron micrograph of Pt nanowires deposited by LP-EBID in a four-point measurement structure. Scale bar indicates 1 $\mu$m.



were removed from the capsules, and atomic force microscope (Molecular Imaging Pico SPM II) images of the large area deposits were acquired to determine the thickness of the deposited material.

Figure 1b shows individual platinum nanodots patterned by liquid-phase EBID. This image was taken through the membrane immediately after patterning. The doses change linearly from 7 pC at the lower left corner through 27 pC at the upper right. Some evidence of deposition can be seen at the three lowest doses (circled); however, there appears to be a threshold near 10 pC at which deposition accelerates. Beyond this dose the dot diameter grows slowly with dose. From 10 to 27 pC the dots increase in diameter from 40 ± 5 to 65 ± 5 nm. Figure 1c shows ~50 nm wide lines patterned into a four-point measurement structure with a linear dose of 2.3 $\mu$C/cm. This image was taken from the backside of the membrane after drying. Thus, even without optimization of the process conditions, LP-EBID has demonstrated sub-50 nm resolution.

Atomic-force microscopy (AFM) imaging was performed in tapping mode to map the morphology of the Pt nanostructures deposited by liquid-phase EBID. Figure 2a depicts one such deposit, which was patterned by raster-scanning the electron beam over an area of a few square micrometers with a step size of 200 nm. The surface of the polyimide membrane was leveled to zero height using image analysis software, and the variations in height (depth) of the patterned nanostructure above (below) the membrane are plotted in Figure 2b for two representative line profiles. Bearing in mind the direction of the lithographic e-beam scan, which ran from right to left and bottom to top relative to Figure 2a, it is evident that the amount of Pt material deposited during a given scan depends in some manner on the cumulative dose of charge delivered by the electron beam. For example, tracing the height variation of Profile 1 in Figure 2 shows that "later" lines in the e-beam scan (i.e., the first two near-horizontal lines of dark spots, close to the start of Profile 1) produced only indentations in the polyimide membrane, whereas the "earlier" scan lines induced the growth of Pt deposits reaching ~100 nm above the membrane (e.g., see Profile 2). This effect can also be observed in the SEM inset in Figure 3b, and it is generally attributed

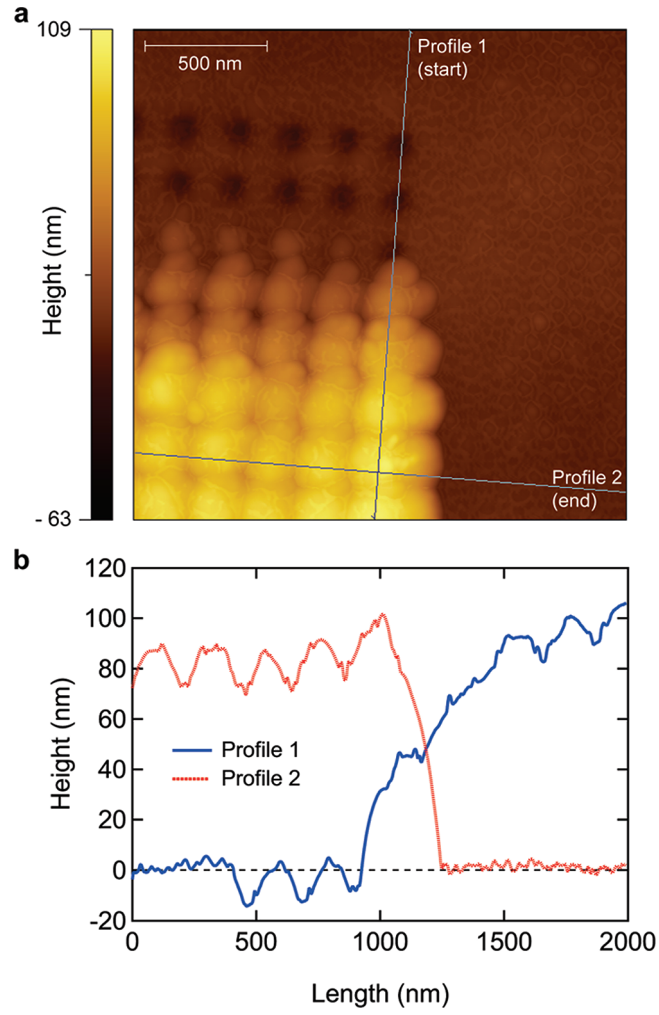


**Figure 2.** (a) Topographic AFM image of nanostructures deposited by liquid-phase EBID on polyimide membrane, showing accumulation of Pt as the lithographic e-beam scan progresses (right to left and bottom to top on the image). Finally, only "dimples" (dark spots) develop, possibly indicative of a nucleation threshold for e-beam-induced Pt growth. (b) Line profiles extracted from the image with distinct "dimples" and "bumps" corresponding to individual lithographically defined steps in the e-beam scan.

to extra deposition on existing structures by secondary-electron spraying from the currently fabricated structure.[10]

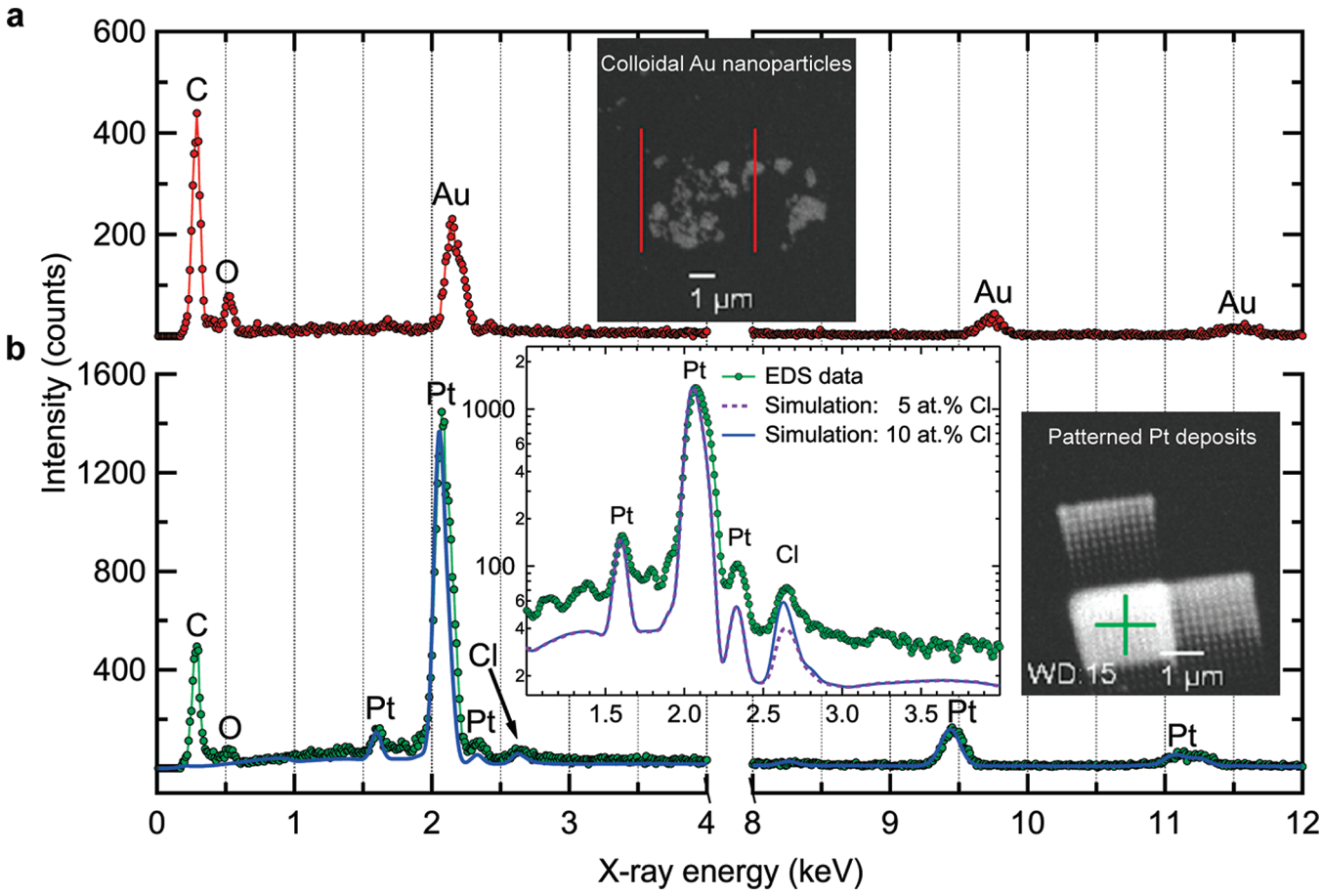


**Figure 3.** (a) Experimental X-ray spectrum of colloidal Au NPs (100 nm diameter) drop-cast onto the polyimide membrane, which is represented by the C and O peaks. Inset: SEM image of patch of Au NPs with vertical lines defining the region for the EDS scan. (b) Experimental X-ray spectrum of Pt deposits on the same polyimide membrane, together with simulated X-ray spectrum of $Pt_{0.9}Cl_{0.1}$ free-standing film (see below). Inset (right): SEM image of patterned deposits with a cross marking the spot from which the EDS spectrum was collected. Inset (middle): Enlarged spectral region around main Pt peak, comparing the experimental data with Monte Carlo simulations of electron-induced X-ray yields from two 100 nm thick free-standing films of $Pt_{(1-x)}Cl_x$, where $x$ corresponds to either 0.05 or 0.10 atomic fraction of Cl; the simulated spectra are normalized to the height of the experimental Pt peak at 2.07 keV.

The origins of the indentions in the polyimide layer are unclear, but the presence of high-contrast features in the electron micrographs, even where only indentations are seen in the AFM image, suggests that Pt is likely imbedded in the membrane.

Once deposition begins, we observe a remarkably high deposition rate for liquid-phase EBID. Taking a modest height of 35 nm (e.g., the shoulder near the midpoint of Profile 1 in Figure 2b) and a dose of 35 mC/cm$^2$ gives 1000 nm of deposit per C/cm$^2$. In contrast, Botman et al. observed a deposition rate from a metal-organic Pt precursor of 50 nm per C/cm$^2$ at the same beam energy.[12] When compared to inorganic precursors, the deposition rate difference is even more pronounced. For example, Wang et al. observed deposition of 2 nm per C/cm$^2$ using $Pt(PF_3)_4$ at a beam energy of 3 kV.[13] Moreover, the metal-organic precursor process resulted in nearly 75% carbon content[12] and the inorganic process in 60% phosphorus content,[13] whereas the material grown by our LP-EBID method is likely to be at least 90% platinum, as evidenced by the X-ray microanalysis described below. And while ion-beam-induced gas-phase deposition of Pt does offer some improvement in purity, the latter still remains at about 30−55% Pt content.[14−18]

We used energy-dispersive X-ray spectroscopy (EDS) at 20 keV to identify the patterned deposits (Figure 3b, right inset) as predominantly platinum, as confirmed in part by the prominence of its combined Mα-M$\beta$ characteristic peak at a little above 2 keV (Figure 3b). Furthermore, the presence of carbon (C) and oxygen (O) Kα peaks in both the spectrum of the patterned deposits and the spectrum of a patch of 100 nm colloidal Au NPs (Figure 3a and inset), which were used as focusing artifacts, indicates that the C and O characteristic X-rays most likely came from the polyimide membrane underlying both the Pt deposits and the Au NPs. Chlorine (Cl), on the other hand, was detected only in the Pt deposits—clearly a byproduct from the dissociation of the Pt:Cl complex in the chloroplatinic acid solution. In order to quantify the amount of Cl contamination in our Pt deposits, we used the NIST DTSA-II software package[19] to perform Monte Carlo simulations of the interactions of energetic electrons with the sample material, including elastic and inelastic scattering events in addition to the generation of characteristic X-rays.

Neglecting the polyimide substrate but specifying the actual detector parameters used in the experiment, the sample

was modeled as a 100 nm thick film of free-standing $Pt_{(1-x)}Cl_x$ with various atomic fractions of Cl, two of which (5 and 10 at. %) are shown in the middle inset of Figure 3b. Despite the relatively rough agreement between experimental and simulated spectra, we can still place a generous upper bound on the amount of incorporated Cl of about 10 at. % by comparing, for example, the heights (within each spectrum) of the Cl peak and the Pt M$\gamma$ peak (near 2.3 keV), or by comparing the integrated Cl peaks (across spectra) after background subtraction. Even if we take into account the considerable uncertainty associated with this particular method of "standardless" EDS analysis, namely that 95% of the results fall within the range of ±50% relative error,[20] the worst-case situation would be 15 at. % Cl and 85 at. % Pt, which is still a marked improvement over either EBID or ion-beam-induced deposition from gas-phase precursors.

This first demonstration of liquid-phase electron-beam-induced deposition reveals many promising aspects of the process and also raises several questions for further investigation. Without any optimization of beam energy, solution composition, or membrane type or thickness, we obtained 40 nm dots (Figure 1b) and 50 nm lines separated by 200 nm (Figure 1c) with platinum purity far exceeding that possible with either organic or inorganic gaseous precursors. The deposition rate was also over an order of magnitude greater than that typically achieved with gas-phase processes. However, several questions need to be answered. In this case, the platinum deposition appears to begin from a pore formed in the polyimide membrane, which may serve to template the deposition and provide high-aspect-ratio structures, but the process may also be undesirable for some applications. Autocatalytic growth from an initial Pt seed in solution may have contributed to the rapid deposition rates observed here, though it may also limit the smallest feature sizes and separations achievable with this technique. Thus, the pore formation and Pt nucleation processes need to be better understood. Likewise, liquid-phase EBID shares some complexity with gas-phase processes as the deposition seems to be dependent on the processing history of the surrounding region. Understanding and compensating for these effects will be important for application of the technique. Finally, for most practical applications, it will be necessary to pattern on a separate substrate placed below the membrane with a well-controlled, liquid-filled gap. Preliminary Monte Carlo simulations suggest that such patterning is possible despite electron scattering in the liquid; however, experimentally implementing such a configuration is challenging. We are currently developing an apparatus to carry out these experiments in addition to exploring deposition on another membrane material (silicon nitride) and with other metals (gold, silver, nickel); if successful, such efforts could open up liquid-phase EBID to a variety of new applications.

**Acknowledgment.** This material is based upon work supported by the Kentucky Science and Engineering Foundation under Grant KSEF-148-502-08-240. Facilities and technical assistance for this work were provided by the University of Kentucky Center for Nanoscale Science and Engineering (CeNSE) and Electron Microscopy Center. The authors thank Larry Rice for his technical assistance with the EDS measurements.

## References

(1) Schossler, C.; Kaya, A.; Kretz, J.; Weber, M.; Koops, H. W. P. *Microelectron. Eng.* **1996**, *30*, 471–474.
(2) Yang, X.; Simpson, M. L.; Randolph, S. J.; Rack, P. D.; Baylor, L. R.; Cui, H.; Gardner, W. L. *Appl. Phys. Lett.* **2005**, *86*, 183106.
(3) Brintlinger, T.; Fuhrer, M. S.; Melngailis, J.; Utke, I.; Bret, T.; Perentes, A.; Hoffmann, P.; Abourida, M.; Doppelt, P. *J. Vac. Sci. Technol. B* **2005**, *23*, 3174–3177.
(4) Croitoru, M. D.; Bertsche, G.; Kern, D. R.; Burkhardt, C.; Bauerdick, S.; Sahakalkan, S.; Roth, S. *J. Vac. Sci. Technol., B* **2005**, *23*, 2789–2792.
(5) Lau, Y. M.; Chee, P. C.; Thong, J. T. L.; Ng, V. *J. Vac. Sci. Technol., A* **2002**, *20*, 1295–1302.
(6) Mukawa, T.; Okada, S.; Kobayashi, R.; Fujita, J.; Ishida, M.; Ichihashi, T.; Ochiai, Y.; Kaito, T.; Matsui, S. *Jpn. J. Appl. Phys. Part 1* **2005**, *44*, 5639–5641.
(7) Liang, T.; Frendberg, E.; Lieberman, B.; Stivers, A. *J. Vac. Sci. Technol., B* **2005**, *23*, 3101–3105.
(8) Randolph, S. J.; Fowlkes, J. D.; Rack, P. D. *Crit. Rev. Solid State Mater. Sci.* **2006**, *31*, 55–89.
(9) Utke, I.; Hoffmann, P.; Melngailis, J. *J. Vac. Sci. Technol., B* **2008**, *26*, 1197–1276.
(10) van Dorp, W. F.; Hagen, C. W. *J. Appl. Phys.* **2008**, *104*, 081301.
(11) Thiberge, S.; Zik, O.; Moses, E. *Rev. Sci. Instrum.* **2004**, *75*, 2280–2289.
(12) Botman, A.; Mulders, J. J. L.; Weemaes, R.; Mentink, S. *Nanotechnology* **2006**, *17*, 3779–3785.
(13) Wang, S.; Sun, Y.-M.; Wang, Q.; White, J. M. *J. Vac. Sci. Technol., B* **2004**, *22*, 1803–1806.
(14) Langford, R. M.; Wang, T. X.; Ozkaya, D. *Microelectron. Eng.* **2007**, *84*, 784–788.
(15) Lin, J. F.; Bird, J. P.; Rotkina, L.; Bennett, P. A. *Appl. Phys. Lett.* **2003**, *82*, 802–804.
(16) Penate-Quesada, L.; Mitra, J.; Dawson, P. *Nanotechnology* **2007**, *18*, 215203.
(17) Tao, T.; Ro, J. S.; Melngailis, J.; Xue, Z. L.; Kaesz, H. D. *J. Vac. Sci. Technol., B* **1990**, *8*, 1826–1829.
(18) Telari, K. A.; Rogers, B. R.; Fang, H.; Shen, L.; Weller, R. A.; Braski, D. N. *J. Vac. Sci. Technol., B* **2002**, *20*, 590–595.
(19) Ritchie, N. W. M. DTSA-II, 1795. http://www.cstl.nist.gov/div837/837.02/epq/dtsa2 (accessed June 1, 2009).
(20) Goldstein, J. *Scanning electron microscopy and x-ray microanalysis*, 3rd ed.; Kluwer Academic/Plenum Publishers: New York, 2003.

NL9012216